applied sciences

MDPI

Article

Attosecond Time Delay in Photoionization of Noble-Gas and Halogen Atoms

Liang-Wen Pi * and Alexandra S. Landsman

Max-Planck-Institut für Physik komplexer Systeme, Nöthnitzer Straße 38, D-01187 Dresden, Germany; landsman@pks.mpg.de

* Correspondence: lwpi@pks.mpg.de; Tel.: +49-351-871-2120

Received: 5 February 2018; Accepted: 20 February 2018; Published: 26 February 2018

Abstract: Ultrafast processes are now accessible on the attosecond time scale due to the availability of ultrashort XUV laser pulses. Noble-gas and halogen atoms remain important targets due to their giant dipole resonance and Cooper minimum. Here, we calculate photoionization cross section, asymmetry parameter and Wigner time delay using the time-dependent local-density approximation (TDLDA), which includes the electron correlation effects. Our results are consistent with experimental data and other theoretical calculations. The asymmetry parameter provides an extra layer of access to the phase information of the photoionization processes. We find that halogen atoms bear a strong resemblance on cross section, asymmetry parameter and time delay to their noble-gas neighbors. Our predicted time delay should provide a guidance for future experiments on those atoms and related molecules.

Keywords: attosecond time delay; giant dipole resonance; Cooper minimum; asymmetry parameter; noble-gas atoms; halogen atoms

1. Introduction

Photoionization processes are traditionally studied using high-resolution synchrotron radiations [1,2], which provides detailed information about the electronic structure of the target. A complete description of photoionization requires information on both the amplitude and phase of the dipole transition matrix elements, through the measurement of cross sections and asymmetry parameter.

Thanks to the development of attosecond XUV-IR laser pump-probe technology [3–5], it is possible to observe and control ultrafast processes in matter on their natural time scale of attoseconds. In general, an electron is ionized from its parent target by absorbing a XUV photon, then the photoelectron's momentum and energy are shifted by the probing IR laser pulse. The time delay between the XUV and IR pulse can be tuned coherently to record the dynamics of electrons from different initial states.

Experimentally, photoionization time delays have been measured for Helium [6], noble-gas atoms [7–11], negative ions [12], molecules [13,14], and condensed matter systems [15,16]. Theoretical description often requires an inclusion of many-electron effects for quantitatively accurate calculations [17–31]. Various aspects of the time delay in single photon ionization have been studied, such as angular dependence [32–35], relativistic effects [36], Attochirp effect [37], and time delay in two photon ionization [38]. Only recently, a well-known discrepancy between theory and experiment on Ne $2p$–$2s$ ionization time delay was resolved [39]. For more details on the attosecond physics of photoionization, a few recent reviews are available [40–43].

Photoionization time delay can be measured using single attosecond XUV pulse in a streaking experiment [44,45], or using attosecond XUV pulse train in a RABBIT experiment (Reconstruction of Attosecond Beating by Interference of Two-photon Transitions) [46]. In the frame of two-photon

perturbation theory [25], both the streaking and RABBIT time delays are decomposed into two parts $\tau = \tau_W + \tau_{CLC}$, where τ_W and τ_{CLC} are the Wigner time delay [47,48] and Coulomb-laser coupling (CLC) time delay, respectively. The Wigner time delay measures the group delay of photoelectron after absorbing an XUV photon, and its accurate calculation frequently requires inclusion of many-electron effects. The CLC time delay is the energy derivative of free-free transition phase following single IR photon absorption. It can be estimated using an analytical formula [25] and does not contain any information about the target structure, as its name suggests.

There has been a number of theoretical and experimental investigations of photoionization time delays from noble-gas atoms in the presence of a giant dipole resonance or a Cooper minimum. However, to the best of our knowledge, detailed theoretical time delay studies on halogen atoms, such as iodine, are not available. The giant dipole resonance is a well-known feature in many atomic photoionization spectra, which is a resonance-like broad peak that occurs above single-photon ionization threshold. It has been interpreted as originating from a potential barrier in a particular one-electron ionization channel [49,50] or as originating from a many-electron, collective oscillation of the atomic electrons [51,52]. Cooper minimum is another feature in many atomic photoionization spectra, which is a cross-section minimum and was explained as being due to a sign change of radial dipole matrix elements as a function of photon frequency [53–55]. In the vicinity of giant dipole resonance or Cooper minimum, the dipole transition matrix element usually undergoes π phase change and results in structured time delay. The giant dipole resonance comes from ionization of core electrons and is therefore known to persist even when the relevant atom becomes part of a larger molecule. For instance, methyl iodide possesses a giant resonance at a similar photon energy as its constituent atom, iodine [56]. Therefore, understanding the giant dipole resonance in non-noble-gas atoms is highly relevant to streaking and RABBIT experiments on molecules, which have only recently become available due to advances in data acquisition and analysis [14]. Moreover, to better understand the nature of the giant dipole resonance, a comparison of Wigner delays between halogen and noble-gas atoms is instructive.

In this paper, we calculate partial photoionization cross sections, asymmetry parameter, phase shift, and Wigner time delay for both noble-gas and halogen atoms. The results are shown in graphs for each pair of neighbor atoms, revealing the great resemblance between the two group. Behaviors of the time delay are discussed for photon energy just above the ionization threshold, in the vicinity of giant resonance and Cooper minimum. In the following sections, we introduce the theoretical methods in Section 2, then present our results in Section 3, reveal the resemblance between noble-gas and halogen atoms, and discuss the features of Wigner time delay near the giant dipole resonance and Cooper minimum. Finally, a conclusion is drawn in Section 4 with possible future work.

2. Overview of Theoretical Methods

We calculate the photoionization dipole transition amplitudes of a neutral atom using the formalism as outlined in the review paper [50]. We will first briefly describe the independent-electron approach using the local-density approximation (LDA), then include the collective effects by TDLDA code provided in Refs. [57,58]. Atomic units ($a.u.$, $\hbar = e = m_e = 1$) are used throughout this paper unless otherwise indicated.

2.1. Independent-Electron Approach

We first choose the photon polarization along the z axis, and calculate the one-photon dipole transition amplitude $\langle \psi_{\mathbf{k}} | z | \psi_0 \rangle$ of the ionization from a bound state ψ_0 to a continuum state $\psi_{\mathbf{k}}$. The magnitude of the photoelectron momentum $\mathbf{k}$ satisfies the energy conservation relation $E \equiv k^2/2 = \omega + \varepsilon_0$, where ω is the photon energy and ε_0 is energy of the initial state.

In the spherical coordinates, one can separate the radial and angular parts of the initial and final states, using the partial-wave expansion:

$$\psi_0(\mathbf{r}) = Y_{l_0 m_0}(\Omega_\mathbf{r}) R_{n_0 l_0}(r), \tag{1}$$

$$\psi_\mathbf{k}(\mathbf{r}) = k^{-1/2} \sum_{lm} \exp\left[-i\left(\sigma_l + \delta_l - \frac{\pi}{2} l\right)\right] Y^*_{lm}(\Omega_\mathbf{k}) R_{El}(r) Y_{lm}(\Omega_\mathbf{r}), \tag{2}$$

where $\sigma_l \equiv \arg\Gamma(l+1-i/k)$ is the Coulomb phase shift, and δ_l is the short-range phase shift (with respect to Coulomb waves) due to the short-range part of the potential. Both the initial and final state wave functions are calculated using the LDA potential and a set of one-electron orbital equations

$$\left[-\frac{1}{2}\nabla^2 + V(\mathbf{r})\right] \psi_i(\mathbf{r}) = \varepsilon_i \psi_i(\mathbf{r}), \tag{3}$$

$$\rho(\mathbf{r}) = \sum_i |\psi_i(\mathbf{r})|^2, \tag{4}$$

$$V(\mathbf{r}) = -\frac{Z}{r} + \int \frac{\rho(\mathbf{r}')}{|\mathbf{r}-\mathbf{r}'|} d\mathbf{r}' + V_{XC}[\rho(\mathbf{r})], \tag{5}$$

where index i runs through occupied orbitals, Z is the atomic number, $\rho(\mathbf{r})$ is the charge density, and V_{XC} is the exchange-correlation functional. Since the exact V_{XC} is unknown, we approximate it with the $X\alpha$ model potential $V_{X\alpha}[\rho(\mathbf{r})] = -3\alpha[\frac{3}{8\pi}\rho(\mathbf{r})]^{1/3}$, in which the exchange parameter α is adopted from Ref. [59]. Equations (3)–(5) are solved iteratively until a self-consistent result is reached.

After integrating over the angular part depending on $\Omega_\mathbf{r}$ and setting its value to A_l, one can obtain the one-photon dipole transition amplitude as follow:

$$\langle \psi_\mathbf{k}|z|\psi_0\rangle = k^{-1/2} \sum_{l=l_0\pm1} A_l Y^*_{lm_0}(\Omega_\mathbf{k}) \exp\left[-i\left(\sigma_l + \delta_l - \frac{\pi}{2} l\right)\right] \langle R_{El}(r)|r|R_{n_0 l_0}(r)\rangle . \tag{6}$$

From here, we calculate cross sections and asymmetry parameter β (see Ref. [50] for detail).

2.2. Inclusion of Collective Effects by Time-Dependent Local-Density Approximation

If collective effects are important, for example, in low-energy ionization of heavy atoms, the single-electron picture is only good as a qualitative description. In the linear response regime, a TDLDA code provided in Refs. [57,58] is employed to calculate the collective effects of an atom in the external dipole field z. A change of charge density $\delta\rho(\mathbf{r};\omega)$ occurs under the influence of the laser field, inducing a change, $\delta V(\mathbf{r};\omega)$, in the potential. Formally, the dipole transition amplitude should be updated as

$$\langle \psi_\mathbf{k}|z|\psi_0\rangle \to \langle \psi_\mathbf{k}|z + \delta V(\mathbf{r};\omega)|\psi_0\rangle , \tag{7}$$

assuming the initial and final state wave functions are still calculated from the LDA potential Equation (5). Both the induced charge density and potential can be solved iteratively from the following equations

$$\delta\rho(\mathbf{r};\omega) = \int \chi_0(\mathbf{r},\mathbf{r}';\omega)\left[z' + \delta V(\mathbf{r}';\omega)\right] d\mathbf{r}', \tag{8}$$

$$\delta V(\mathbf{r};\omega) = \int \frac{\delta\rho(\mathbf{r}';\omega)}{|\mathbf{r}-\mathbf{r}'|} d\mathbf{r}' + \left.\frac{\partial V_{XC}[\rho(\mathbf{r}')]}{\partial\rho(\mathbf{r}')}\right|_{\mathbf{r}'=\mathbf{r}} \delta\rho(\mathbf{r};\omega). \tag{9}$$

In the above equation, $\chi_0(\mathbf{r},\mathbf{r}';\omega)$ is the susceptibility in the independent-electron approximation. It is constructed from the single-electron orbitals

$$\chi_0(\mathbf{r},\mathbf{r}';\omega) = \sum_i \psi^*_i(\mathbf{r})\psi_i(\mathbf{r}') G(\mathbf{r},\mathbf{r}';\varepsilon_i+\omega) + \sum_i \psi_i(\mathbf{r})\psi^*_i(\mathbf{r}') G^*(\mathbf{r},\mathbf{r}';\varepsilon_i-\omega), \tag{10}$$

where i runs over the occupied states and G is the Green's function that satisfies the equation

$$\left[\frac{1}{2}\nabla^2 - V(\mathbf{r}) + E\right] G(\mathbf{r},\mathbf{r}';E) = \delta(\mathbf{r}-\mathbf{r}'). \tag{11}$$

The Green's function can be expanded in the spherical basis:

$$G(\mathbf{r},\mathbf{r}';E) = \sum_{lm} G_l(r,r';E) Y^*_{lm}(\Omega_{\mathbf{r}}) Y_{lm}(\Omega_{\mathbf{r}'}), \tag{12}$$

where the radial part $G_l(r,r';E)$ satisfies the radial equation

$$\left[\frac{1}{2}\frac{\partial^2}{\partial r^2} + \frac{1}{r}\frac{\partial}{\partial r} - V(r) - \frac{l(l+1)}{2r^2} + E\right] G_l(r,r';E) = \frac{\delta(r-r')}{r^2}. \tag{13}$$

Letting $j_l(r;E)$ and $h_l(r;E)$ be the regular and irregular solution to the homogeneous version of Equation (13), one can construct the radial component of the Green's function as

$$G_l(r,r';E) = \frac{j_l(r_<;E) h_l(r_>;E)}{W[j_l,h_l]}, \tag{14}$$

where $r_<$ ($r_>$) refers to the smaller (larger) one between r and r'. The Wronskian $W[j_l,h_l]$ is defined as

$$W[j_l,h_l] \equiv \frac{1}{2}r^2\left[j_l(r)\frac{dh_l(r)}{dr} - h_l(r)\frac{dj_l(r)}{dr}\right]_{r=a}, \tag{15}$$

which is independent of an arbitrary distance a. In practice, both the regular and irregular functions $j_l(r;E)$ and $h_l(r;E)$ are solved numerically.

In summary, the collective effects of a many-electron atom are included as a frequency-dependent induced potential $\delta V(\mathbf{r};\omega)$. It was shown in Ref. [57] that this induced potential has the same angular part $Y_{10}(\Omega_{\mathbf{r}})$ as the external dipole field z, which enables us to perform an angular decomposition of the dipole transition amplitude as follows

$$\begin{aligned}\langle\psi_{\mathbf{k}}|z+\delta V(\mathbf{r};\omega)|\psi_0\rangle =& k^{-1/2}\sum_{l=l_0\pm1} A_l Y^*_{lm_0}(\Omega_{\mathbf{k}}) \exp\left[-i\left(\sigma_l+\delta_l-\frac{\pi}{2}l\right)\right] \\ &\times\left\langle R_{El}(r)|r+\delta V(r;\omega)|R_{n_0l_0}(r)\right\rangle, \qquad (16)\\ =& k^{-1/2}\sum_{l=l_0\pm1} A_l Y^*_{lm_0}(\Omega_{\mathbf{k}}) \exp\left[-i\left(\sigma_l+\delta_l+\eta_l-\frac{\pi}{2}l\right)\right] \\ &\times\left|\left\langle R_{El}(r)|r+\delta V(r;\omega)|R_{n_0l_0}(r)\right\rangle\right|, \qquad (17)\end{aligned}$$

where the induced potential $\delta V(r;\omega)$ is a complex function in general and contributes a induced phase shift $\eta_l \equiv -\arg\left\langle R_{El}(r)|r+\delta V(r;\omega)|R_{n_0l_0}(r)\right\rangle$ to the radial integration.

We solve the LDA potential Equation (5) and the induced potential Equation (9) using the code provided in Ref. [58]. The Wigner time delay, which is the energy derivative of the dipole transition phase, is calculated as

$$\tau_W = \frac{d}{dE}\arg\langle\psi_{\mathbf{k}}|z+\delta V|\psi_0\rangle. \tag{18}$$

For a linearly polarized laser, the most probable ionization is along the z direction and hence $m_0 = 0$. The dipole transition amplitude is evaluated for $\Omega_{\mathbf{k}} = 0$ or integrated on $\Omega_{\mathbf{k}}$ over a solid angle that depends on how the photoelectron spectrum is measured in the experiment.

3. Results and Discussion

In this section, we present our calculations of partial photoionization cross sections, asymmetry parameters, phase shifts, and Wigner time delay for noble-gas and halogen atoms. The similarity

between the two groups is revealed, and Wigner time delay in the vicinity of giant dipole resonance and Cooper minimum is discussed.

3.1. General Features

Figures 1 and 2 shows the results for three outermost subshells of xenon, iodine, krypton, and bromine atoms, while Figure 3 shows that for two outermost subshells of argon and chlorine atoms. Our first impression is the great similarity between any two neighbor atoms on the periodic table, which is not a surprise due to their similar electron configurations. Another reason is that in the LDA approximation, the multiplet splitting of the halogen atoms is not included. The LDA potential is a mean-field potential only depending on the radial wave functions R_{nl}, which indicates spherical symmetry for the target atoms. However, due to electron interactions, open-shell atoms (like halogen) don't have exact spherical symmetry and there will be an energy splitting among different ionic states. For example, the singly-ionized iodine configuration $5s^2 5p^4$ has three ionic states ^3P, ^1D, and ^1S, whose energy splitting is shown in Table 1 of Ref. [60]. Even though the LDA potential can not resolve the energy splitting, it still provides valuable results for the halogen atoms. This is because for deeply-bound subshells, the energy splitting is much smaller than its binding energy, which suggests spherical symmetry is not a bad approximation. The partial photoionization cross sections can be seen as a total cross sections from all the ionic states, while the asymmetry parameters, phase shifts, and Wigner time delay can be treated as average values among the different ionic states.

For noble-gas atoms, both their partial cross sections and asymmetry parameters presented in Figures 1–3 agree well with other theoretical and experimental data (Ref. [61] and references there in). For halogen atoms, our calculations also have good qualitative agreement with Ref. [62]. More comparison is available for iodine atom in Refs. [60,63–65].

The asymmetry parameter β measures the channel interference effects for the photoionization process. In the central-potential model, β for photoionization of an electron with initial orbital angular momentum l_0 is given by the Cooper-Zare formula [66]

$$\beta = \frac{l_0(l_0-1)P_{l_0}^2 + (l_0+1)(l_0+2) - 6l_0(l_0+1)P_{l_0}\cos\Delta}{(2l_0+1)\left[l_0 P_{l_0}^2 + (l_0+1)\right]}, \tag{19}$$

$$P_{l_0} = \frac{\left|\left\langle R_{El_0-1}(r)\middle|r+\delta V(r;\omega)\middle|R_{n_0l_0}(r)\right\rangle\right|}{\left|\left\langle R_{El_0+1}(r)\middle|r+\delta V(r;\omega)\middle|R_{n_0l_0}(r)\right\rangle\right|}, \tag{20}$$

$$\Delta = \sigma_{l_0+1} - \sigma_{l_0-1} + \delta_{l_0+1} - \delta_{l_0-1} + \eta_{l_0+1} - \eta_{l_0-1}, \tag{21}$$

where P_{l_0} is the ratio of the radial dipole transition amplitude and Δ is the phase different between two channels. Since β depends on the phase difference Δ, it provides an accuracy check of our phase shift calculations by comparing with other available theoretical and experimental values. There are two cases in which β does not depends on Δ or only depends on it weakly, thus it does not provide direct access to the phase shift. First, within LDA approximation, the s subshell has only one ionization channel $ns \to \varepsilon p$, thus $P_{l_0} = 0$ and its asymmetry parameter is a constant (not shown in all the figures). It is known that the asymmetry parameter for s subshell will depends on energy if including the initial-state correlations, spin-orbit and other relativistic interactions [67–69]. Secondly, at the Cooper minimum, one ionization channel dominates and the channel interference effects are weak. In most of the cases, Cooper minimum appears in the $l_0 \to l_0+1$ channel, therefore $P_{l_0} \to \infty$ and $\beta \to \frac{l_0-1}{2l_0+1}$ shows weak dependence on Δ.

Since Wigner time delay is an energy derivative of dipole transition phase, it is important to examine the behavior of the phase shifts for a better understanding of Wigner time delay. The short-range phase shift, δ_l, plus induced phase shift, η_l, are plotted in the third row of all figures. Only the phase shifts of $l_0 \to l_0+1$ channel are shown because this is where the interesting giant resonance and Cooper minimum happens. The phase shifts of $l_0 \to l_0-1$ channel just decrease

monotonically. We did not plot the Coulomb phase shift σ_l due to its known analytical form and trivial behavior. It increases quickly within 10 eV above the ionization threshold, then slowly approaches zero at higher photon energy. The dramatic increase of the Coulomb phase shift near the threshold, has a great impact on the Wigner time delay. As shown in the fourth row of all figures, Wigner time delays tend to be infinity near the threshold, because of the large positive energy derivative of the Coulomb phase shift.

In all the graphs of Figure 1, there are spikes located roughly at 63 eV, 140 eV and 180 eV for Xe, and 50 eV, 120 eV and 165 eV for iodine. These are resonances generated from excited Rydberg states when the ionization channels are opened for the 4*d*, 4*p* and 4*s* subshells. Since Rydberg resonances are not the focus of this paper, we have removed some of the resonance data points to smooth the curve. Spikes appearing in Figures 2 and 3 have the same origin.

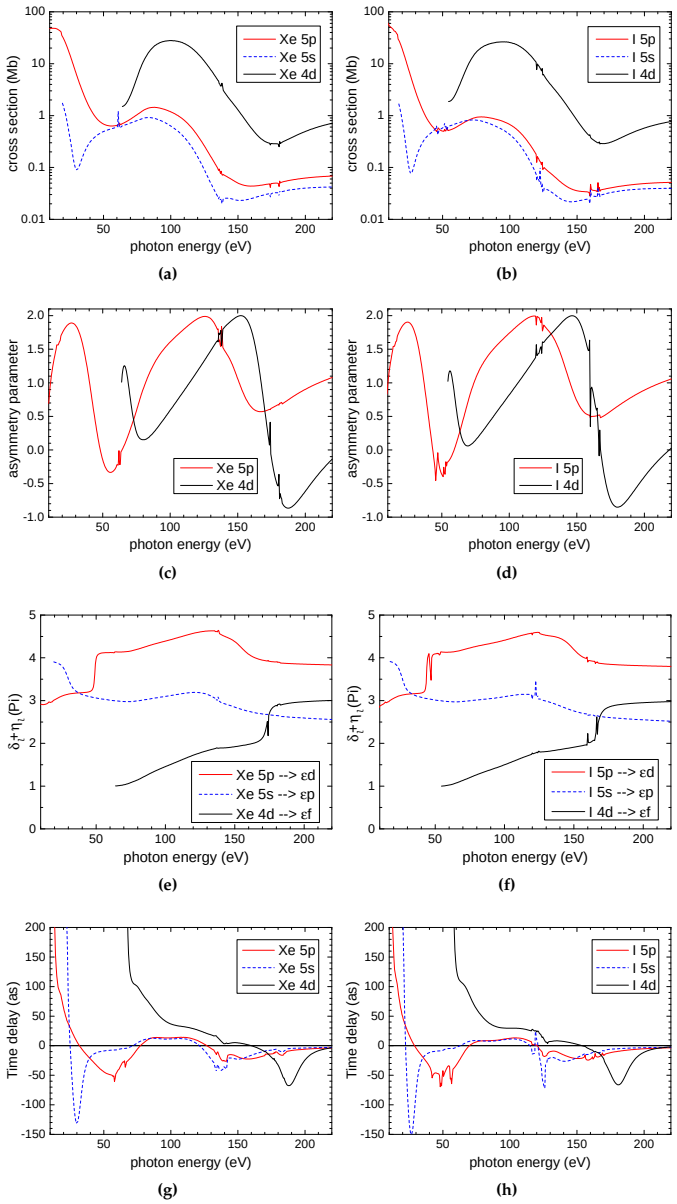

Figure 1. Left to right columns: calculations for xenon (**a**,**c**,**e**,**g**) and iodine (**b**,**d**,**f**,**h**) atoms. Top to bottom rows: partial cross section (**a**,**b**), asymmetry parameter (**c**,**d**), short-range plus induced phase shift (**e**,**f**), and Wigner time delay (**g**,**h**) for subshells 5*p*, 5*s* and 4*d*.

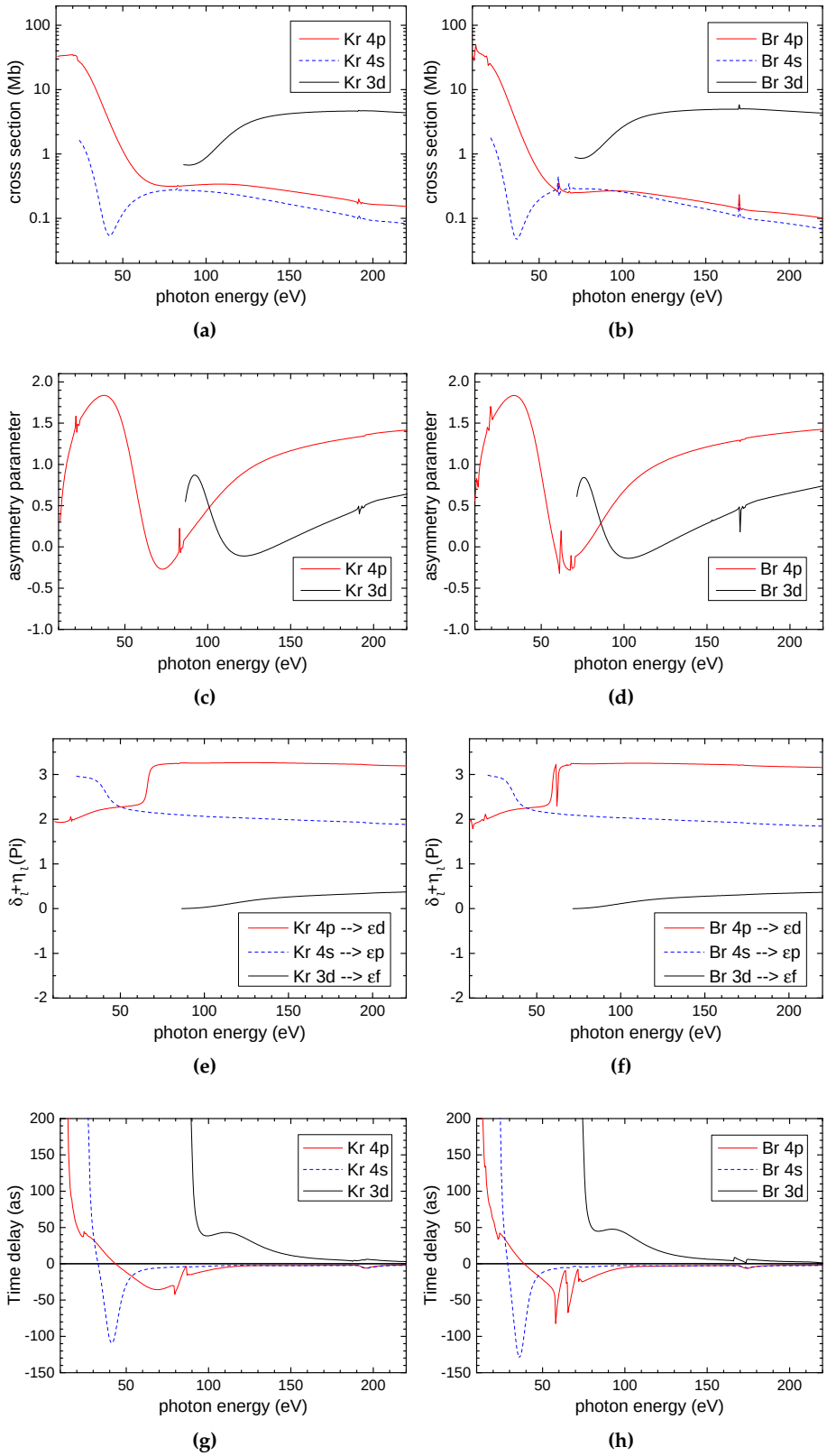

Figure 2. Left to right columns: calculations for krypton (**a**,**c**,**e**,**g**) and bromine (**b**,**d**,**f**,**h**) atoms. Top to bottom rows: partial cross section (**a**,**b**), asymmetry parameter (**c**,**d**), short-range plus induced phase shift (**e**,**f**), and Wigner time delay (**g**,**h**) for subshells 4*p*, 4*s* and 3*d*.

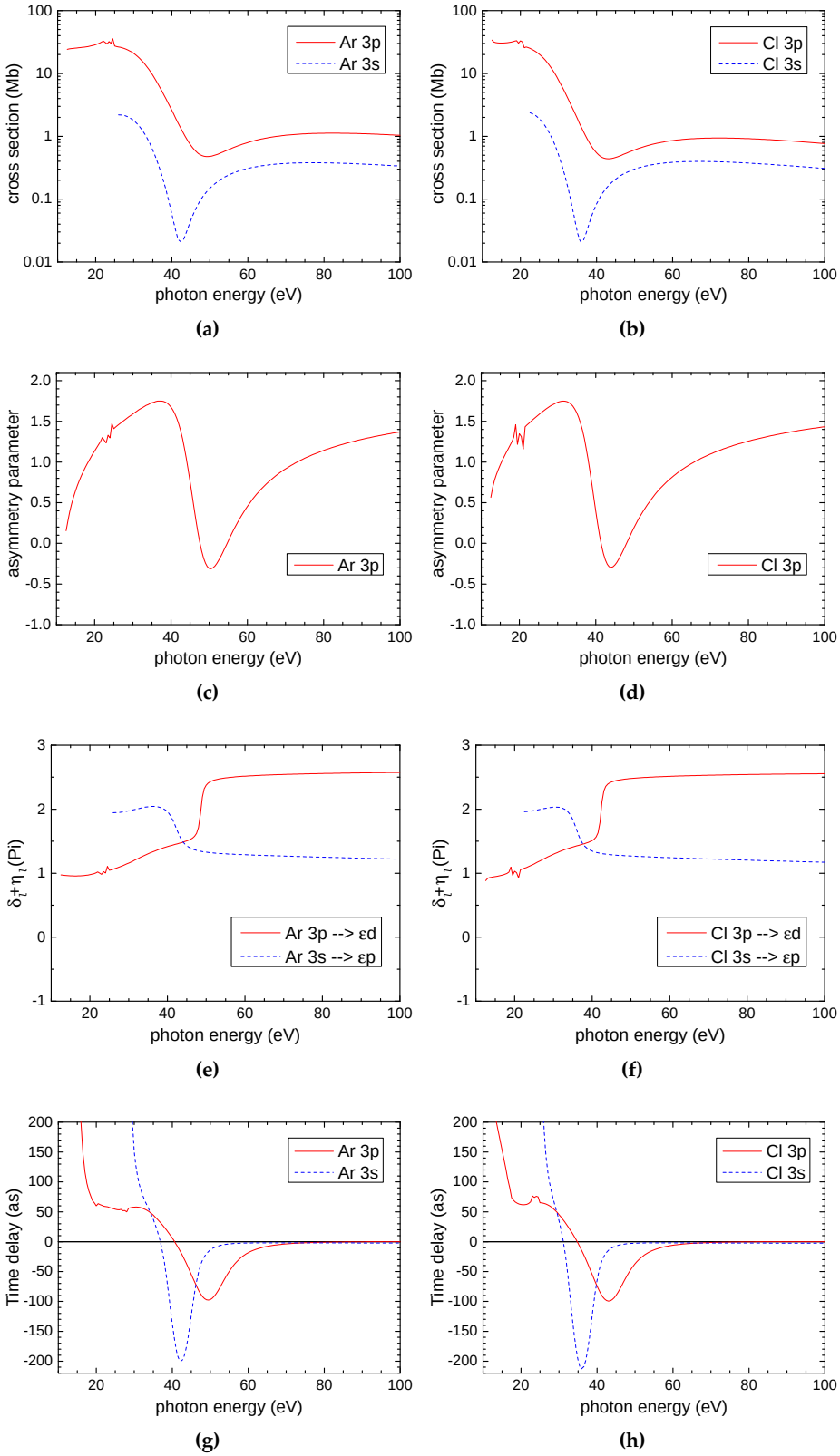

Figure 3. Left to right columns: calculations for argon (**a**,**c**,**e**,**g**) and chlorine (**b**,**d**,**f**,**h**) atoms. Top to bottom rows: partial cross section (**a**,**b**); asymmetry parameter (**c**,**d**); short-range plus induced phase shift (**e**,**f**); and Wigner time delay (**g**,**h**) for subshells 3*p* and 3*s*.

3.2. Phase Shift and Time Delay in the Vicinity of Giant Resonance and Cooper Minimum

In this section, we discuss the general features of the Wigner time delay for noble-gas and halogen atoms. A simple observation of the bottom row of Figures 1–3 suggests that one can divide the time delay into three parts based on the photon energy. Within about 10 eV above the photoionization threshold, all Wigner time delays show large positive values and decrease dramatically due to the dominant Coulomb phase shift explained in the previous section. For photon energy larger than 200 eV in Figures 1 and 2, or 70 eV in Figure 3, the phase shift (third row in all figures) becomes constant and structureless, thus the time delay goes to zero. The photon energy range from tens of eV to a few hundred eV is where the giant resonance and Cooper minimum happens, and we will discuss how these cross section features affect the time delay.

Let us first investigate Figure 1 for Xe and I atoms. The calculations for these two atoms look very similar. The following discussion applies to both of them and we will not distinguish them unless it is necessary. A resonance, including the Cooper minimum, usually means a phase change of π. The broad $4d$ giant resonance Figure 1a,b is dominated by the $4d \rightarrow \varepsilon f$ channel and stretches roughly from 60–160 eV. Within the same photon energy range, the phase shift of $4d \rightarrow \varepsilon f$ channel increases approximately at a constant slope from π to 2π, as shown in Figure 1e,f. Since the Wigner time delay is the energy derivative of the phase shift, we can estimate the time delay in the giant resonance regime using the average phase change slope

$$\tau_W = \frac{\text{phase change } \pi}{\text{energy change of 100 eV}} = \frac{\pi}{3.675\ a.u.} = 0.855\ a.u. = 21\ as. \tag{22}$$

The calculated time delay Figure 1g,h decreases slowly across the giant resonance regime and is about 30 *as* at the resonance peak 100 eV. The estimated 21 *as* is therefore not too far off from the calculation. In Figure 1a,b, the ionization cross sections of $5p$ and $5s$ subshells also have giant resonances due the interchannel interaction with $4d$ subshell. Across the giant resonance energy range from 70 to 110 eV, Wigner time delays of $5p$ and $5s$ subshells in Figure 1g,h shows plateaus of roughly 10 *as*, corresponding to a monotonic phase change across the giant resonance regime.

Besides giant resonance, Cooper minimum is also accompanied by a π phase change. In Figure 1e,f, there are two Cooper minima at 50 and 150 eV for the $5p \rightarrow \varepsilon d$ channel, and one Cooper minimum at 170 eV for the $4d \rightarrow \varepsilon f$ channel. The width of these minima is much narrower than the giant resonance but still has a π phase change. One would expect large value (negative or positive) Wigner time delay. But these dramatic phase changes does not contribute much to the time delay, because the decreased angular momentum channels $5p \rightarrow \varepsilon s$ and $4d \rightarrow \varepsilon p$ dominate the ionization cross section and have a monotonically-decreased phase shift (not shown in the figure), which will generate moderate-value negative time delays. Our calculated time delays in Figure 1g,h support the above analysis, showing negative sinks at the Cooper minimum regime. At both Cooper minima, 50 eV for the $5p \rightarrow \varepsilon d$ channel and 170 eV for the $4d \rightarrow \varepsilon f$ channel, the phase shifts quickly increase by π, indicating large positive time delay, but the actual time delays are about -50 *as* due to the dominance of $l_0 \rightarrow l_0 - 1$ channels. In the vicinity of Cooper minimum, while the sign of time delay is determined by the $l_0 \rightarrow l_0 - 1$ channels, the width of the negative time delay sinks reflect the width of the Cooper minimum. For example, in the $5p \rightarrow \varepsilon d$ channel, the phase shift shows a wider Cooper minimum at 150 eV than at 50 eV, thus the time delay sink at 150 eV is broader.

The time delay in ionization from xenon and iodine $5s$ subshell is determined by a single ionization channel $5s \rightarrow \varepsilon p$. The $5s$ time delay shows a deep narrow negative sink at 30 eV, and a shallow broad negative sink at 130 eV, which are both determined by the phase shift at the Cooper minima. However, as mentioned previously, the LDA approximation is unable to reproduce the β parameter deviations at the Cooper minima [67–69], which raises concerns about the qualitative accuracy of current phase shift calculations for s subshell. In order to reproduce the correct β parameter and phase shift, one needs to include the initial-state correlations and relativistic effects.

The cross section, β parameter, phase shift and time delay calculations for krypton, bromine, argon and chlorine are presented in Figures 2 and 3. When the atoms become lighter, the dependence of these quantities on photon energy becomes less structured compared to xenon and iodine. Except the Kr 3*d* cross section shows a very broad giant resonance, ionizations from other subshells just contain a single Cooper minimum. The behavior of time delay near the vicinity of giant resonance and Cooper minimum is similar to the case of xenon and iodine.

4. Conclusions

In conclusion, we have calculated partial photoionization cross sections, asymmetry parameter, phase shift, and Wigner time delay for both noble-gas and halogen atoms, finding great similarity between these two groups in the presence of the giant dipole resonance. Our calculated cross sections and asymmetry parameters agree well with other theoretical and experimental values. Wigner time delay presents a flat plateau across the giant resonance regime, due to its slow and monotonic phase change. Near the Cooper minimum, the Wigner time delay forms a negative sink, because the $l_0 \rightarrow l_0 - 1$ channel with decreasing phase dominates. If the breakdown of spherical symmetry is considered, Wigner time delay should be calculated for different ionic states of halogen atoms. For photoionization from *s* subshells, the TDLDA method is not able to reproduce the right asymmetry parameters near the Cooper minimum. Future studies including the initial-state correlations and relativistic effects should give the right asymmetry parameters and different time delays for these cases as well. Our predicted time delays should be useful for future experiments on those atoms and related molecules.

Acknowledgments: A.S.L. acknowledges funding from the Max Planck Center for Attosecond Science (MPC-AS).

Author Contributions: L.-W.P. performed the calculations; L.-W.P. and A.S.L. analyzed the data and wrote the paper.

Conflicts of Interest: The authors declare no conflict of interest.

Abbreviations

The following abbreviations are used in this manuscript:

as	attosecond (10^{-18} s)
a.u.	atomic units
CLC	Coulomb-laser coupling
IR	Infrared
RABBIT	Reconstruction of attosecond harmonic beating by interference of two-photon transitions
(TD)LDA	(Time-dependent) local-density approximation
XUV	extreme ultraviolet

References

1. Schmidt, V. Photoionization of atoms using synchrotron radiation. *Rep. Prog. Phys.* **1992**, *55*, 1483.
2. Becker, U.; Shirley, D.A. (Eds.) *VUV and Soft X-ray Photoionization*; Springer: Boston, MA, USA, 1996.
3. Drescher, M.; Hentschel, M.; Kienberger, R.; Tempea, G.; Spielmann, C.; Reider, G.A.; Corkum, P.B.; Krausz, F. X-ray Pulses Approaching the Attosecond Frontier. *Science* **2001**, *291*, 1923–1927.
4. Hentschel, M.; Kienberger, R.; Spielmann, C.; Reider, G.A.; Milosevic, N.; Brabec, T.; Corkum, P.; Heinzmann, U.; Drescher, M.; Krausz, F. Attosecond metrology. *Nature* **2001**, *414*, 509–513.
5. Paul, P.M.; Toma, E.S.; Breger, P.; Mullot, G.; Augé, F.; Balcou, P.; Muller, H.G.; Agostini, P. Observation of a Train of Attosecond Pulses from High Harmonic Generation. *Science* **2001**, *292*, 1689–1692.
6. Ossiander, M.; Siegrist, F.; Shirvanyan, V.; Pazourek, R.; Sommer, A.; Latka, T.; Guggenmos, A.; Nagele, S.; Feist, J.; Burgdörfer, J.; et al. Attosecond correlation dynamics. *Nat. Phys.* **2017**, *13*, 280–285.
7. Schultze, M.; Fiess, M.; Karpowicz, N.; Gagnon, J.; Korbman, M.; Hofstetter, M.; Neppl, S.; Cavalieri, A.L.; Komninos, Y.; Mercouris, T.; et al. Delay in photoemission. *Science* **2010**, *328*, 1658–1662.

8. Klünder, K.; Dahlström, J.M.; Gisselbrecht, M.; Fordell, T.; Swoboda, M.; Guénot, D.; Johnsson, P.; Caillat, J.; Mauritsson, J.; Maquet, A.; et al. Probing Single-Photon Ionization on the Attosecond Time Scale. *Phys. Rev. Lett.* **2011**, *106*, 143002.
9. Guénot, D.; Klünder, K.; Arnold, C.L.; Kroon, D.; Dahlström, J.M.; Miranda, M.; Fordell, T.; Gisselbrecht, M.; Johnsson, P.; Mauritsson, J.; et al. Photoemission-time-delay measurements and calculations close to the 3s-ionization-cross-section minimum in Ar. *Phys. Rev. A* **2012**, *85*, 053424.
10. Palatchi, C.; Dahlström, J.M.; Kheifets, A.S.; Ivanov, I.A.; Canaday, D.M.; Agostini, P.; DiMauro, L.F. Atomic delay in helium, neon, argon and krypton. *J. Phys. B At. Mol. Opt. Phys.* **2014**, *47*, 245003.
11. Sabbar, M.; Heuser, S.; Boge, R.; Lucchini, M.; Carette, T.; Lindroth, E.; Gallmann, L.; Cirelli, C.; Keller, U. Resonance Effects in Photoemission Time Delays. *Phys. Rev. Lett.* **2015**, *115*, 133001.
12. Lindroth, E.; Dahlström, J.M. Attosecond delays in laser-assisted photodetachment from closed-shell negative ions. *Phys. Rev. A* **2017**, *96*, 013420.
13. Haessler, S.; Fabre, B.; Higuet, J.; Caillat, J.; Ruchon, T.; Breger, P.; Carré, B.; Constant, E.; Maquet, A.; Mével, E.; et al. Phase-resolved attosecond near-threshold photoionization of molecular nitrogen. *Phys. Rev. A* **2009**, *80*, 011404.
14. Huppert, M.; Jordan, I.; Baykusheva, D.; von Conta, A.; Wörner, H.J. Attosecond Delays in Molecular Photoionization. *Phys. Rev. Lett.* **2016**, *117*, 093001.
15. Locher, R.; Castiglioni, L.; Lucchini, M.; Greif, M.; Gallmann, L.; Osterwalder, J.; Hengsberger, M.; Keller, U. Energy-dependent photoemission delays from noble metal surfaces by attosecond interferometry. *Optica* **2015**, *2*, 405–410.
16. Tao, Z.; Chen, C.; Szilvasi, T.; Keller, M.; Mavrikakis, M.; Kapteyn, H.; Murnane, M. Direct time-domain observation of attosecond final-state lifetimes in photoemission from solids. *Science* **2016**, *353*, 62–67.
17. Moore, L.R.; Lysaght, M.A.; Parker, J.S.; van der Hart, H.W.; Taylor, K.T. Time delay between photoemission from the 2p and 2s subshells of neon. *Phys. Rev. A* **2011**, *84*, 061404.
18. Zhang, C.H.; Thumm, U. Streaking and Wigner time delays in photoemission from atoms and surfaces. *Phys. Rev. A* **2011**, *84*, 033401.
19. Caillat, J.; Maquet, A.; Haessler, S.; Fabre, B.; Ruchon, T.; Salières, P.; Mairesse, Y.; Taïeb, R. Attosecond Resolved Electron Release in Two-Color Near-Threshold Photoionization of N_2. *Phys. Rev. Lett.* **2011**, *106*, 093002.
20. Sukiasyan, S.; Ishikawa, K.L.; Ivanov, M. Attosecond cascades and time delays in one-electron photoionization. *Phys. Rev. A* **2012**, *86*, 033423.
21. Nagele, S.; Pazourek, R.; Feist, J.; Burgdörfer, J. Time shifts in photoemission from a fully correlated two-electron model system. *Phys. Rev. A* **2012**, *85*, 033401.
22. Dahlström, J.M.; L'Huillier, A.; Maquet, A. Introduction to attosecond delays in photoionization. *J. Phys. B At. Mol. Opt. Phys.* **2012**, *45*, 183001.
23. Dahlström, J.M.; Carette, T.; Lindroth, E. Diagrammatic approach to attosecond delays in photoionization. *Phys. Rev. A* **2012**, *86*, 061402.
24. Pazourek, R.; Feist, J.; Nagele, S.; Burgdörfer, J. Attosecond Streaking of Correlated Two-Electron Transitions in Helium. *Phys. Rev. Lett.* **2012**, *108*, 163001.
25. Dahlström, J.; Guénot, D.; Klünder, K.; Gisselbrecht, M.; Mauritsson, J.; L'Huillier, A.; Maquet, A.; Taïeb, R. Theory of attosecond delays in laser-assisted photoionization. *Chem. Phys.* **2013**, *414*, 53–64.
26. Kheifets, A.S. Time delay in valence-shell photoionization of noble-gas atoms. *Phys. Rev. A* **2013**, *87*, 063404.
27. Feist, J.; Zatsarinny, O.; Nagele, S.; Pazourek, R.; Burgdörfer, J.; Guan, X.; Bartschat, K.; Schneider, B.I. Time delays for attosecond streaking in photoionization of neon. *Phys. Rev. A* **2014**, *89*, 033417.
28. Magrakvelidze, M.; Madjet, M.E.A.; Dixit, G.; Ivanov, M.; Chakraborty, H.S. Attosecond time delay in valence photoionization and photorecombination of argon: A time-dependent local-density-approximation study. *Phys. Rev. A* **2015**, *91*, 063415.
29. Magrakvelidze, M.; Madjet, M.E.A.; Chakraborty, H.S. Attosecond delay of xenon 4d photoionization at the giant resonance and Cooper minimum. *Phys. Rev. A* **2016**, *94*, 013429.
30. Magrakvelidze, M.; Chakraborty, H. Attosecond time delays in the valence photoionization of xenon and iodine at energies degenerate with core emissions. *J. Phys. Conf. Ser.* **2017**, *875*, 022015.
31. Shields, D.; De, R.; Madjet, M.; Manson, S.T.; Chakraborty, H. Photoionization of open-shell halogen atoms endohedrally confined in C_{60}. *J. Phys. Conf. Ser.* **2017**, *875*, 042004.

32. Dahlström, J.M.; Lindroth, E. Study of attosecond delays using perturbation diagrams and exterior complex scaling. *J. Phys. B At. Mol. Opt. Phys.* **2014**, *47*, 124012.
33. Wätzel, J.; Moskalenko, A.S.; Pavlyukh, Y.; Berakdar, J. Angular resolved time delay in photoemission. *J. Phys. B At. Mol. Opt. Phys.* **2015**, *48*, 025602.
34. Heuser, S.; Jiménez Galán, Á.; Cirelli, C.; Marante, C.; Sabbar, M.; Boge, R.; Lucchini, M.; Gallmann, L.; Ivanov, I.; Kheifets, A.S.; et al. Angular dependence of photoemission time delay in helium. *Phys. Rev. A* **2016**, *94*, 063409.
35. Ivanov, I.A.; Kheifets, A.S. Angle-dependent time delay in two-color XUV+IR photoemission of He and Ne. *Phys. Rev. A* **2017**, *96*, 013408.
36. Saha, S.; Mandal, A.; Jose, J.; Varma, H.R.; Deshmukh, P.C.; Kheifets, A.S.; Dolmatov, V.K.; Manson, S.T. Relativistic effects in photoionization time delay near the Cooper minimum of noble-gas atoms. *Phys. Rev. A* **2014**, *90*, 053406.
37. Goldsmith, C.; Jaroń-Becker, A.; Becker, A. Effect of attochirp on attosecond streaking time delay in photoionization of atoms. *J. Phys. B At. Mol. Opt. Phys.* **2018**, *51*, 025601.
38. Su, J.; Ni, H.; Jaroń-Becker, A.; Becker, A. Time Delays in Two-Photon Ionization. *Phys. Rev. Lett.* **2014**, *113*, 263002.
39. Isinger, M.; Squibb, R.J.; Busto, D.; Zhong, S.; Harth, A.; Kroon, D.; Nandi, S.; Arnold, C.L.; Miranda, M.; Dahlström, J.M.; et al. Photoionization in the time and frequency domain. *Science* **2017**, *358*, 893–896.
40. Pazourek, R.; Nagele, S.; Burgdörfer, J. Attosecond chronoscopy of photoemission. *Rev. Mod. Phys.* **2015**, *87*, 765–802.
41. Calegari, F.; Sansone, G.; Stagira, S.; Vozzi, C.; Nisoli, M. Advances in attosecond science. *J. Phys. B At. Mol. Opt. Phys.* **2016**, *49*, 062001.
42. Krausz, F. The birth of attosecond physics and its coming of age. *Phys. Scr.* **2016**, *91*, 063011.
43. Ciappina, M.F.; Pérez-Hernández, J.A.; Landsman, A.S.; Okell, W.A.; Zherebtsov, S.; Förg, B.; Schötz, J.; Seiffert, L.; Fennel, T.; Shaaran, T.; et al. Attosecond physics at the nanoscale. *Rep. Prog. Phys.* **2017**, *80*, 054401.
44. Itatani, J.; Quéré, F.; Yudin, G.L.; Ivanov, M.Y.; Krausz, F.; Corkum, P.B. Attosecond Streak Camera. *Phys. Rev. Lett.* **2002**, *88*, 173903.
45. Eckle, P.; Pfeiffer, A.N.; Cirelli, C.; Staudte, A.; Dörner, R.; Muller, H.G.; Büttiker, M.; Keller, U. Attosecond Ionization and Tunneling Delay Time Measurements in Helium. *Science* **2008**, *322*, 1525–1529.
46. Muller, H. Reconstruction of attosecond harmonic beating by interference of two-photon transitions. *Appl. Phys. B* **2002**, *74*, s17–s21.
47. Wigner, E.P. Lower Limit for the Energy Derivative of the Scattering Phase Shift. *Phys. Rev.* **1955**, *98*, 145–147.
48. Smith, F.T. Lifetime Matrix in Collision Theory. *Phys. Rev.* **1960**, *118*, 349–356.
49. Fano, U.; Cooper, J.W. Spectral distribution of atomic oscillator strengths. *Rev. Mod. Phys.* **1968**, *40*, 441–507.
50. Starace, A.F. Theory of atomic photoionization. In *Handbuch der Physik*; Mehlhorn, W., Ed.; Springer: Berlin, Germany, 1982; Volume 31, pp. 1–121.
51. Wendin, G. Collective effects in atomic photoabsorption spectra. III. Collective resonance in the $4d^{10}$ shell in Xe. *J. Phys. B At. Mol. Phys.* **1973**, *6*, 42–61.
52. Amusia, M.; Cherepkov, N.A. Many-electron Correlations in Scattering processes. *Case Stud. At. Phys.* **1975**, *5*, 47–179.
53. Bates, D.R. The Quantal Calculation of the Photo-Ionization Cross-Section of Atomic Potassium. *Proc. R. Soc. Lond.* **1947**, *188*, 350–357.
54. Seaton, M.J. A Comparison of Theory and Experiment for Photo-Ionization Cross-Sections. II. Sodium and the Alkali Metals. *Proc. R. Soc. Lond. A* **1951**, *208*, 418–430.
55. Cooper, J.W. Photoionization from outer atomic subshells. A model study. *Phys. Rev.* **1962**, *128*, 681–693.
56. Lindle, D.W.; Kobrin, P.H.; Truesdale, C.M.; Ferrett, T.A.; Heimann, P.A.; Kerkhoff, H.G.; Becker, U.; Shirley, D.A. Inner-shell photoemission from the iodine atom in CH_3I. *Phys. Rev. A* **1984**, *30*, 239–244.
57. Zangwill, A.; Soven, P. Density-functional approach to local-field effects in finite systems: Photoabsorption in the rare gases. *Phys. Rev. A* **1980**, *21*, 1561–1572.
58. Zangwill, A.; Liberman, D.A. A nonrelativistic program for optical response in atoms using a time-dependent local density approximation. *Comput. Phys. Commun.* **1984**, *32*, 63–73.

59. Schwarz, K. Optimization of the Statistical Exchange Parameter α for the Free Atoms H through Nb. *Phys. Rev. B* **1972**, *5*, 2466–2468.
60. Farnoux, F.C.; Amar, M.B. Inner and outer shell ionization for atomic iodine: Calculation of cross-sections and angular distribution parameters. *J. Electron Spectrosc. Relat. Phenom.* **1986**, *41*, 67–87.
61. Becker, U.; Shirley, D.A. Partial Cross Sections and Angular Distributions. In *VUV and Soft X-ray Photoionization*; Becker, U., Shirley, D.A., Eds.; Springer: Boston, MA, USA, 1996; pp. 135–180.
62. Manson, S.T.; Msezane, A.; Starace, A.F.; Shahabi, S. Photoionization of chalcogen and halogen atoms: Cross sections and angular distributions. *Phys. Rev. A* **1979**, *20*, 1005–1018.
63. Amusia, M.Y.; Cherepkov, N.A.; Chernysheva, L.V.; Manson, S.T. Photoionization of atomic iodine and its ions. *Phys. Rev. A* **2000**, *61*, 020701.
64. Domondon, A.T.; Tong, X.M. Photoabsorption spectra of I and its ions in the 4d region. *Phys. Rev. A* **2002**, *65*, 032718.
65. Chen, Z.; Msezane, A.Z. Random-phase approximation with exchange for the inner-shell electron transitions. *Phys. Rev. A* **2005**, *72*, 050702.
66. Cooper, J.; Zare, R.N. Angular Distribution of Photoelectrons. *J. Chem. Phys.* **1968**, *48*, 942–943.
67. Manson, S.T.; Starace, A.F. Photoelectron angular distributions: Energy dependence for s subshells. *Rev. Mod. Phys.* **1982**, *54*, 389–405.
68. Kutzner, M.; Radojević, V.; Kelly, H.P. Extended photoionization calculations for xenon. *Phys. Rev. A* **1989**, *40*, 5052–5057.
69. Tulkki, J. Multiple excitation at xenon 5s photoionization threshold. *Phys. Rev. Lett.* **1989**, *62*, 2817–2820.